Author's Accepted Manuscript

www.elsevier.com/locate/pss

Ionospheric Photoelectrons at Venus: Case Studies and First Observation in the Tail

S.M.E. Tsang, A.J. Coates, G.H. Jones, R.A. Frahm, J.D. Winningham, S. Barabash, R. Lundin, A. Fedorov

PII: S0032-0633(15)00020-3
DOI: http://dx.doi.org/10.1016/j.pss.2015.01.019
Reference: PSS3908

To appear in: *Planetary and Space Science*

Received date: 14 March 2014
Revised date: 11 September 2014
Accepted date: 27 January 2015

Cite this article as: S.M.E. Tsang, A.J. Coates, G.H. Jones, R.A. Frahm, J.D. Winningham, S. Barabash, R. Lundin, A. Fedorov, Ionospheric Photoelectrons at Venus: Case Studies and First Observation in the Tail, *Planetary and Space Science*, http://dx.doi.org/10.1016/j.pss.2015.01.019

Ionospheric Photoelectrons at Venus: Case Studies and First Observation in the Tail

S.M.E. Tsang[a,b], A.J. Coates[a,b,*], G. H. Jones[a,b], R.A. Frahm[c], J.D. Winningham[c], S. Barabash[d], R. Lundin[d], A. Fedorov [e]

[a] *Mullard Space Science Laboratory, University College London, Surrey RH5 6NT, U.K.*

[b] *The Centre for Planetary Sciences at UCL/Birkbeck, Gower Street, London WC1E 6BT, U.K.*

[c] *Southwest Research Institute, San Antonio, TX 78228-0510, U.S.A.*

[d] *Swedish Institute of Space Physics, Box 812, SE-981 28 Kiruna, Sweden*

[e] *Centre d'Etude Spatiale des Rayonnements 9 av. Du Colonel Roche, BP 44346, 31028 Toulouse Cedex 4, France*

* Corresponding author: Phone +44-1483-204145, Fax +44 1483 278312, email a.coates@ucl.ac.uk

Abstract

The presence of photoelectrons in ionospheres, including that of unmagnetised Venus, can be inferred from their characteristic spectral peaks in the electron energy spectrum. The electrons within the peaks are created by the photoionisation of neutrals in the upper atmosphere by the solar HeII 30.4nm line. Here, we present some case studies of photoelectron spectra observed by the ASPERA-4 instrument aboard Venus Express with corresponding ion data. In the first case study, we observe photoelectron peaks in the sunlit ionosphere, indicating relatively local production. In the second case study, we observe broadened peaks in the sunlit ionosphere near the terminator, which indicate scattering processes between a more remote production region and the observation point. In the third case study, we present the first observation of ionospheric photoelectrons in the induced magnetotail of Venus, which we suggest is due to the spacecraft being located at that time on a magnetic field line connected to the dayside ionosphere at lower altitudes. Simultaneously,

low energy ions are observed moving away from Venus. In common with observations at Mars and at Titan, these imply a possible role for the relatively energetic electrons in producing an ambipolar electric field which enhances ion escape.

Keywords:

Venus, ionosphere, photoelectrons, solar wind, escape

1. Introduction

Ionospheric photoelectrons are usually observed in sunlit ionospheres. They have been observed in several solar system contexts, including Earth (e.g. Coates *et al*., 1985), Mars (Frahm *et al*., 2006a), Titan (e.g. Coates *et al*., 2007), in Saturn's ring ionosphere (Coates *et al*., 2005) and in Saturn's inner magnetosphere (Schippers *et al*., 2009). When observed, they usually indicate local production of photoelectrons, but may also be indicative of a magnetic connection to regions where ionisation is occurring (e.g. Coates *et al*., 1985, Frahm *et al*., 2006b, Coates *et al*., 2007).

The first observation of distinct ionospheric photoelectron peaks by the ESA Venus Express spacecraft (VEx) was found in data from 18 May 2006 (Coates *et al*., 2008). The ionospheric electron component of the plasma is characterized by a high peak of electron flux occurring mainly due to solar photoionisation below 60eV. This flux is relatively intense compared to the background. The solar spectrum contains discrete spectral lines (see example solar spectrum in Gibson, 1973). In the ionosphere of Venus, the dominant solar EUV helium line at 30.4 nm causes photoionisation of atmospheric carbon dioxide and atomic oxygen, yielding electrons that populate a narrow energy range of the electron spectrum (e.g. Mantas and Hanson, 1979). The analysis by Coates *et al*. (2008) indicated that

the photoelectrons observed by VEx were mainly due to ionisation of oxygen at altitudes lower than the spacecraft and subsequently transported to the observation point.

Similar ionospheric photoelectrons have been observed at Mars (mainly from the ionisation of CO_2, Frahm *et al.*, 2006a,b) and at Titan (from ionisation of N_2, Coates *et al.*, 2007). At Titan, photoelectrons observed in the tail on Cassini's T9 encounter were used to infer a magnetic connection to the sunlit ionosphere at lower altitude (Coates *et al.*, 2007), which was supported by a comparison of the magnetometer data with an MHD model showing that magnetic connection was indeed possible in that case (Wei *et al.*, 2007). Similar photoelectron peaks are also observed in the tail region of Mars (Frahm *et al.*, 2006a) inferring magnetic connection to Mars and transport from the Martian dayside ionosphere (Liemohn, *et al.*, 2006).

The theory of photoelectron generation at Venus is similar to that detailed for Mars by Mantas and Hanson (1979). For Venus, there are two main species (carbon dioxide and atomic oxygen) interacting with the 30.4 nm HeII solar line, each generating a multiple of possible parent states and ejecting electrons as described in equations 1 and 2 below.

$$CO_2 + h\upsilon \rightarrow {CO_2}^+ + e^- \begin{cases} X^2\Pi_g \; ionisation\; potential\; 13.8eV \rightarrow 27.0eV\; electron \\ A^2\Pi_u \; ionisation\; potential\; 17.7eV \rightarrow 23.1eV\; electron \\ B^2{\Sigma_u}^+ \; ionisation\; potential\; 18.1eV \rightarrow 22.7eV\; electron \\ C^2{\Sigma_g}^+ \; ionisation\; potential\; 19.4eV \rightarrow 21.4eV\; electron \end{cases} \quad (1)$$

(Padial *et al.*, 1981)

$$O + h\upsilon \rightarrow O^+ + e^- \begin{cases} {}^4S\; ionisation\; potential\; 13.62eV \rightarrow 27.16eV\; electron \\ {}^2D\; ionisation\; potential\; 17.10eV \rightarrow 23.68eV\; electron \\ {}^2P\; ionisation\; potential\; 18.50eV \rightarrow 22.28eV\; electron \end{cases} \quad (2)$$

(Mantas and Hanson, 1979)

Because atomic oxygen is the dominant species at ionospheric altitudes near the exobase at ~200 km (Fox and Bougher, 1991; Fox and Sung, 2001), the photoelectron population observed at Venus Express altitudes (250-700 km in the Coates et al., 2008 case) is dominated by the atomic oxygen source (Coates *et al*. (2008)). In particular, models have shown that detailed modelling of the Venus atmosphere can generate electron spectra showing electron flux peaks in the 22-24 and 27eV range (McCormick *et al.*, 1976; Cravens *et al*., 1980; Knudsen *et al*., 1980; Spenner *et al*., 1997).

Peaks in the electron spectrum generated near the exobase must have a conduit in order for them to be transported in altitude to the point of observation without changing their energy spectrum. This conduit is the magnetic field (c.f. Coates et al., 1985, Frahm et al., 2006a,b, Coates et al., 2007).

Pioneer Venus Orbiter (PVO) observations have shown that there is no intrinsic magnetic field at Venus (Slavin *et al.*, 1980; Russell *et al.*, 1980; Phillips *et al.*, 1987). There is, however, an induced magnetosphere caused by the interaction of the solar wind with the outer atmosphere of the planet. The interaction causes the solar wind magnetic field to be draped around Venus (Luhmann and Cravens, 1991; Law and Cloutier, 1995). In our region of interest, the draped field lines may be connected to the dayside ionosphere at times. The draping region is complex with an intermediate boundary called the magnetic barrier, or plasma mantle (Spenner *et al.*, 1997) or transition region (Coates et al., 2008). PVO observed the solar wind interaction with Venus but the resolution of the electron measurements was insufficient to reveal the photoelectron peaks (e.g. Knudsen *et al.*, 1980 and the model comparisons shown in Spenner *et al*., 1997). The VEx ASPERA-4 ELS is the first instrument which has observed peaks in the ionospheric electron spectrum. This is a

result of the ~8% energy resolution and the differential measurements performed by ELS as described below.

A detailed comparison of a multi-stream kinetic model with ASPERA-ELS photoelectron data was performed by Cui *et al.* (2011). The comparison indicated good agreement between the observed and modelled photoelectron peak energies and flux decrease features, and fair agreement between the observed and modelled absolute fluxes when the magnetic field direction is included.

In this paper, we present clear evidence for ionospheric photoelectrons in the tail of Venus, indicating that there exists, at times, magnetic connectivity between the dayside Venus ionosphere and its tail.

2. Instrument

VEx was launched on 09 November 2005. It arrived at Venus on 11 April 2006. The spacecraft payload comprises seven experiments, including ASPERA-4, the Analyzer of Space Plasma and EneRgetic Atoms (Barabash *et al*., 2007). The ASPERA-4 experiment is composed of four instruments, two of which measure neutral particles (the Neutral Particle Detector, NPD, and the Neutral Particle Imager, NPI), one measuring ions (the Ion Mass Analyzer, IMA), and one measuring electrons (the ELectron Spectrometer, ELS).

The ELS measures the electron population near Venus between 0.8eV and 30,000eV. The lowest energy of observation is dependent on the charging of the spacecraft. The spacecraft potential in turn, depends on the flux of the local electrons in the plasma, and the characteristic energy of the plasma. These values change as VEx orbits and samples various plasma regions from a 66,000km apoapsis to a periapsis in the 250-350 km range (see Titov

et al., 2006). During its sampling of the electron plasma around Venus, we have used the ELS to search for evidence of ionospheric photoelectrons.

The data used in this paper come from the ELS and IMA instruments of the ASPERA-4 experiment (Barabash *et al.*, 2007). The electron-optical design of the ELS is a top hat analyser and collimator system with a nominal 360° x 4° field of view (Barabash *et al.*, 2007). Small non-concentric differences between the ELS sectors occurred during manufacture causing slight sector differences (Collinson *et al.*, 2009) which are compensated for by the instrument calibration. A scanner enables increased angular coverage so that ELS sweeps out the entire sky; however, about a quarter of the sky is blocked by the spacecraft. Particles enter the instrument through a collimator, passing a set of baffles which confine the incoming electrons. This baffling system includes a very effective light trap. Electrons of a particular energy are selected by applying a voltage to the inner hemisphere corresponding to the energy divided by the analyser k-factor, with the outer hemisphere at ground. Any electrons of lower or higher energies than the energy passband (~8% $\Delta E/E$ at FWHM) will impact the sides of the hemispheres and not pass through to the detector. The selected electrons which traverse the inner hemisphere gap impact a microchannel plate (MCP) detection system via a programmable decoupler screen. Each incoming electron is multiplied by the MCP, causing the impact of ~10^6 electrons onto a discrete anode. The anode at which they are measured corresponds to the particle entering at the opposite side of the instrument. There are 16 anodes on ELS, each designed to cover a 22.5° portion of the 360° azimuthal field of view. For the observations shown in this paper, ELS sweeps through 127 logarithmically spaced steps, covering the complete range of energies from 0.8 to 30,000eV in 4s. Data from anode 11 is presented here as it is one of the least affected by obscuration by, and photoemission of, electrons from the spacecraft.

The ASPERA-4 IMA instrument (Barabash et al., 2007) is an electrostatic-magnetic momentum analyser covering an energy range from 10 to 36,000eV. There are three stages to the electrostatics: (1) incoming ions are elevation analysed within the angular range of ±45° degrees (about every 5.6°), (2) electrostatic deflection through a top-hat analyser energy filters the ions, and (3) ions are then accelerated into the magnetic section. The magnetic section is an orange-segment arrangement causing momentum deflection in the radial direction, resulting in mass discrimination up to about 40 amu. IMA accumulates ion counts in bins of 16 elevation angles, 16 azimuthal angles, 32 mass channels and 96 energies every 192 seconds. In this paper, as well as ion spectrograms summed over all sectors, we present pitch angle distributions of O^+ organized parallel and perpendicular to the magnetic field (e.g. Figure 2(d). We also show energy-angle plots (e.g. Fig 2(e)). Due to the geometry of the IMA, the mass bin boundaries appear in a non-linear way in these plots (see Barabash et al., 2007 for more detail).

3. Case Studies

Data from the first five months of the mission were examined to identify candidate ionospheric photoelectron events. Within the time period analysed, photoelectrons are always seen in the sunlit ionosphere, and ionospheric plasma is sometimes seen in the Venus tail, including one example (shown here) of characteristic ionospheric photoelectron energy peaks observed in the tail. Three representative case studies are presented, all from June 2006, including the tail observation. Electron data from the ELS is used to indicate the presence of the photoelectrons. Ion data from the IMA are used to search for possible related ion outflow.

3.1. 30 June 2006

Figure 1a shows the VEx orbit on 30 June 2006 (day of year, DOY 181) in Venus Solar Orbital (VSO) co-ordinates where X_{vso} is the direction towards the Sun, Y_{vso} is in the direction opposing the planet's orbital motion about the Sun and Z_{vso} completes the right-handed set. The x-axis shows the X_{vso} co-ordinate and the y-axis shows the cylindrical radial distance from the Sun-Venus line calculated from $\rho=\sqrt{(y^2+z^2)}$. For this period, Venus Express's orbital plane was close to being perpendicular to the Sun-Venus line; throughout its orbit, the sub-spacecraft point, therefore, remained close to the terminator. The Sun is to the left of the figure and model positions for Venus' bow shock and ionopause are shown as the blue and green lines respectively (Biernat *et al*., 1999, 2000; Luhmann *et al.,* 1992).

Electron data taken during the time period shown in Figure 1a can be seen in Figure 2a. At the beginning of the plot, the spacecraft is in the solar wind, crossing the bow shock at ~01:25 UT. The upstream solar wind was quiet with a low speed (<400kms^{-1}). It remains similar during the event and the downstream solar wind conditions are similar to those of the upstream solar wind. The spacecraft remains in the Venus sheath until ~01:48 UT, when a transition region between the sheath and the ionosphere is seen, containing plasma characteristic of both (c.f. Coates *et al*, 2008). That is, the ionosphere, made up of low energy electrons, and the sheath, comprising high energy electrons, coexist at the same spatial and temporal location. In the sheath region (~01:25-01:48 UT), a lower energy peak (<20eV) is seen in addition to the main peak (starting at ~100eV). We interpret this as being associated with differential charging on the spacecraft. The ionosphere is entered at ~01:50UT.

Detailed electron spectra show that there are two distinct peaks as seen in Figure 1b, at 16eV and 21eV, between 01:52 and 01:56 UT in the Venus ionosphere region. Note that a two-peaked energy distribution is seen in each of the unobscured ELS anodes 6-11 in the ELS data at this time. We suggest (following Frahm *et al*., 2006a and Coates *et al.* 2008) that these correspond to the two peaks of ionospheric photoelectrons at 21-24 and 27eV expected from theory (Mantas and Hanson, 1979) but shifted by a negative potential in the Venus ionosphere. This allows us to infer a negative potential of ~-6V at this time, part of this may be spacecraft potential but the full potential would include any field-aligned potential. The Solar Zenith Angle (SZA), shown in Figure 2c, during the observation is 88° within the ionosphere segment and up to 90° within the transition regions. The altitude (shown in Figure 2(c)) during the observation is 346km – 350km. In Figure 1b, the electron energy spectrum is averaged over 20 spectra and the spectral shape is sustained continually throughout the feature. The two ionospheric photoelectron peaks thus clearly have high statistical significance in this case compared to the background electron population.

The IMA data (Figure 2b) shows high energy (~100-1000eV) thermalised solar wind ions throughout the sheath region and low energy (<30eV) O^+ ions in the ionosphere (see Figure 2e, simultaneous with the ionospheric photoelectron observations. In the ion spectrogram the pulsed appearance (with 192s repetition period) is caused by the electrostatic elevation scanning of the instrument field of view through the ion population. When the magnetic field direction is considered, the bulk of the ions are seen to be moving away from Venus as revealed by the ion velocity space contour shown in Figure 2d.

This case represents data acquired from a terminator pass through the Venus ionosphere. Both the photoelectrons and low energy ions are observed to be approximately

symmetric with respect to the pericentre. Photoelectron peaks are clearly observed for the SZA of 88° in this region.

Mantas and Hanson (1979) predicted that the ionospheric photoelectrons would produce two distinct peaks. These are expected at 21-24eV and 27eV, when CO_2 or O in the atmosphere is ionised by the 30.4nm HeII line. The 21eV peak in the figure is interpreted as the anticipated 27eV peak, indicating a negative potential. This peak is smaller than the lower energy peak, consistent with its interpretation as the anticipated 21-24eV peak. Assuming that the theory is correct, and if any field-aligned potential is relatively small, the spacecraft potential can be inferred from the difference in energy between the expected peak and the observed peak. Using this technique, a negative potential is estimated during the ionosphere part of the orbit as ~-6V, consistent with both peaks in Figure 1b. The negative potential inferred for Case Study 1 is somewhat more negative compared to the electron temperature in this region (~few eV), which might be expected to determine the spacecraft potential (e.g. Whipple *et al.*, 1981). However it is possible that this value also includes a field aligned potential. In the high density ionosphere, the ionospheric plasma, electrons are more mobile than in lower density regions. They then dominate the flux of particles to and from the spacecraft, including spacecraft photoelectrons. This leads to a negative potential during ~01:30-02:00U.T. The energetic ionospheric photoelectrons are still observed even though the potential is negative. The ions observed are mostly O^+.

Case study 1 includes an interesting example of spacecraft charging. Outside the ionosphere, the spacecraft is sunlit and photoelectrons dominate the current balance leading to a positive spacecraft potential. Photoelectrons are then trapped close to the spacecraft, due to the positive potential. This effect is more important during some orbits than others. In case studies 1 and 3 we infer that the spacecraft potential must be above +10 V during the

observation of the low energy (<10eV) secondary peaks, or 'beams', seen in the sheath region, which we suggest is due to differential charging. A spacecraft potential in this range is not unknown as potentials of up to +30 V have been seen at Saturn with the Cassini spacecraft (e.g. Lewis *et al*., 2008). Charging can be affected by both input flux and by orientation. One of the reasons for the differential charging could be that part of the spacecraft is in shadow whilst the rest in not. Similar electron beams associated with charging have been seen occasionally in the Cassini data (e.g. Rymer *et al*., 2001) and frequently in the Cluster and Double Star data at Earth (Szita *et al*., 2001; Fazakerley *et al*., 2005).

The ionospheric photoelectrons are observed in this case study while the solar zenith angle (SZA) is 88°, i.e. within the sunlit ionosphere.

3.2. 04 June 2006

Figure 3(a) shows the VEx orbit on 04 June 2006 (DOY 155) in a similar format to Figure 1(a). VEx crosses the bow shock from upstream on the sunlit side of Venus. The pericentre of the orbit is close to the terminator. This case represents one where the spacecraft travels from local noon towards midnight.

Electron and ion data taken during the time period shown in Figure 3(a) can be seen in Figure 4(a),(b) (which is presented in a similar format to Figure 2(a),(b). The top panel of Figure 4(a) shows the electron spectrogram, 4(b) shows the positive ions seen with IMA, and 4(c) shows the altitude of the spacecraft.

As before, at the start of the interval VEx is in the solar wind, which is more disturbed than in the previous case study and it also has a low speed. Some pick up ions can be seen in

the upstream region as these are away from the central solar wind beam (within the first 192 s elevation scan). The electron data indicate multiple bow shock crossings as there are several intensifications before reaching the magnetosheath. This could be a quasi-parallel shock or a change in the solar wind. Nothing unusual is seen in the ACE or WIND data at Earth, the nearest solar wind plasma monitor.

VEx initially crosses the bow shock at ~01:25 UT, remaining in the Venus sheath until ~01:35 UT, when the ionosphere is observed. Only one, relatively broad, ionospheric photoelectron peak is identified in the sunlit ionosphere region between 01:36 and 01:42 UT at ~18eV by a detailed spectrum from the ionosphere (shown in Figure 3b). This single peak is seen instead of the two distinct peaks as shown in Case Study 1. This single peak is relatively broad in energy and is most likely due to energy cascading caused by continuous slowing (Jasperse, 1977). A detailed energy spectrum from the tail region is shown in Figure 3(c). The tail region population is observed between 01:52-01:54 UT and 01:55-01:57 UT. These two intervals include the observation of electron populations which are reminiscent of the generic ionospheric electron population. Fairly constant intensities are observed during both the main ionosphere and the tailward ionospheric-type populations. This would suggest that the production of the photoelectrons occurs below the spacecraft and that they are then transported to the spacecraft (c.f. Coates et al., 2008). It also implies that the spacecraft potential did not change within the energy acceptance of the instrument. Since the peaks in the electron spectrum dominate the electron spectrum and they are caused by the single ionization of an ion/atom, they are most likely generated where the ion concentration is high. The highest concentration of such ions is deeper in the ionosphere, so the electrons are most likely escaping from the exobase of the planet.

The simultaneous positive ion data (Figure 4(b)) shows low (<30eV) energy O^+ ions in the ionosphere with some evidence for a correlation with the fluxes of ionospheric electrons. In figure 4(d) and (e), the ion pitch angle distribution is shown as the ion distribution function in the plane containing the magnetic field and velocity vectors. A detailed examination of the ion data shows that the O^+ planetary ions are seen to flow away from Venus during the tail example (Figure 4(e)).

In figure 4(f) and (g), ion composition data are shown. The vertical axis is ion energy and the horizontal axis is position of ions on the detector surface. Red curves correspond, from left to right, to O_2^+, O^+, He^+, H^+. Some H^+ contamination is present in the spectrum of Figure 4(f) and it overlaps the O^+ signature so the O^+ signature is not as clear as in previous examples; however, the O^+ signature can clearly be observed in Figure 4(g). The observed O^+ ions are of planetary origin.

During the observation of ionospheric photoelectrons, only one peak is visible, which is indicative of broadening of the peaks in energy. Such a broadening has also been seen at Mars (Frahm *et al.*, 2009). A possible explanation of the broadening could be associated with some instability of the particle distribution function (which has a positive slope with energy) or due to magnetic field fluctuations between the production and observation points. These effects may also broaden the pitch angle distribution. In the source photoelectron distributions (e.g. Case Study 1, 30 June 2006) there is a positive slope in the electron distribution function. Instabilities driven by this positive slope could cause waves which would interact with the population to cause broadening, assuming that there is enough distance (and time) between the original distribution and the observation point for instabilities to develop and waves to occur; a broadening of the distribution may be the result.

In Case Study 2, there are two intervals of electron populations, reminiscent of the generic ionosphere, observed in the tail, with corresponding positive ion flux visible in the IMA data. These data show that the composition of the ions in these tail observations is mostly O^+. This agrees with our suggestion (c.f. Coates *et* al., 2008) of ionisation of particles below the spacecraft. These ions are clearly field aligned in the IMA pitch angle plots (Figure 2d and Figures 4 d and e). The relatively energetic ionospheric electron population, escaping along a field line, would give rise to ambipolar diffusion by pulling out the ions (e.g. Coates *et al*., 2007, Ganguli 1996, Yau et al., 2007 and references therein). The ions in the IMA data may be drawn out of the ionosphere by an ambipolar electric field, which may also affect the photoelectron peak location.

3.3. 03 June 2006

Figure 5(a) shows the VEx orbit on 03 June 2006 (DOY 154) in a similar format to Figure 1(a). Again, VEx traverses the bow shock from the sunlit side of Venus. Pericentre of the orbit is very close to the terminator. This pass represents another case where the spacecraft is orbiting from local noon towards midnight.

The ELS and IMA data taken during the time period are shown in Figure 6(a) and (b). As in Figure 1, the top panel Figure 6(a) shows the electron spectrogram, the second panel, 6(b), shows the IMA positive ions data. The third panel, Figure 6(c), shows the spacecraft altitude.

At the beginning of the plot, VEx is in the solar wind. The solar wind is not as disturbed as Case Study 2 but more so than Case Study 1. It has a speed of approximately $400 kms^{-1}$. The downstream solar wind conditions are similar to the upstream conditions.

However, the exit bow shock crossing is 30 minutes later than on other days which are similar, indicating that the tail of Venus is extended.

VEx crosses the bow shock at ~01:25 UT. The spacecraft remains in the Venus sheath until ~01:36 UT, when a transition region between the sheath and the ionosphere is seen. In the sheath region, a lower energy peak (<20eV) is seen in addition to the main peak (starting at ~100eV). We interpret this as associated with differential charging on the spacecraft. VEx enters the ionosphere at ~01:38 UT.

An ionospheric photoelectron peak is observed in the sunlit ionosphere between 01:38-01:46 UT at 16 and 18eV. As in the previous example, broadening of the photoelectron peak has occurred, as shown in Figure 5(b). Spacecraft photoelectrons can be seen near the inner edge of the sheath and in the transition region between the inbound bow shock and the ionosphere. Two further intervals of ionospheric plasma are observed in the tail regions between 01:55-01:57 UT (18eV) and 01:58-01:59 UT (18eV), close to the dark ionosphere. These are interpreted to be the 21-24eV photoelectrons, after allowing for a potential correction (3-6eV). This correction is similar to that necessary for the interpretation of Case study 1. The SZA for these tail region ionospheric photoelectrons is between 128° - 130°.

Some ions are seen in the vicinity of the tail region photoelectrons. Ions with energies of 40-50eV are seen between the ionosphere and the tail observations but not during the tail photoelectron observations themselves. In all observations of data within this case study, the electrons and ions are seen to flow away from Venus.

The ionospheric photoelectrons that we observe in the tail region are in the same energy bin as the observations of this ionospheric population in the sunlit ionosphere,

indicating that the spacecraft potential is very similar and that any field aligned potential is small. The observation suggests a magnetic connection to the dayside ionosphere, such that a conduit is available for electrons to quickly be transported to the measured location before the photoelectron peaks can substantially degrade.

This observed ionospheric plasma in the tail region, including the characteristic photoelectron peaks, is highly reminiscent of that observed on the dayside (e.g. Case Study 1). The spacecraft potential is driven negative by the high plasma density in this region as well. At this time, the spacecraft is outside of the shadow of Venus but behind the terminator. The spacecraft cylindrical radial distance from the centre of the tail must be less than one Venus radius (R_v) for VEx to be in shadow. Here, it is more than $1R_v$ indicating that the spacecraft is sunlit. However, the high SZA shows that it is behind the terminator.

Some ions with energies up to approximately 60eV are observed in the vicinity of the tail region photoelectrons, between the ionosphere and the tail electron observation, but both are not simultaneously observed. These ions are shown to be O^+ which are field aligned. The ions could be pulled out by the ambipolar electric field and then gyrate, increasing their energy *via* the pickup process. These ions probably originate in the ionosphere, as they are moving in a field-aligned direction away from the planet, and thus could be further accelerated. The reason for the lack of ions at the time of the tail observation is most likely due to the differing look directions of ELS and IMA, meaning that they sample different pitch angles. IMA itself is not part of the ASPERA-4 Main Unit (MU) but mounted on the opposite side of the spacecraft from the MU, where the scanner spin axis is parallel to the instrument symmetry axis of IMA (the central measurement plane of IMA is perpendicular to the rotating measurement plane of ELS). At the time of the observations, the MU scanner was switched on at a position of 109°, rather than the nominal 90° position. Thus the fields of

view of ELS anode 11 and IMA differ. ELS anode 11 sees a pitch angle range of 15.8° to 29.3° during the first tail observation. Due to noise and obscuration of several of the ELS anodes, data from those that are in a similar look direction to the IMA instrument are unavailable (see Collinson *et al*., 2009, for more information on ELS anodes). ELS and IMA are mounted on the spacecraft in such a way that at the normal scanner position, they are perpendicular to each other.

The ELS pitch angles show near field-alignment of ionospheric photoelectrons in the tail. We suggest that the tail region observations of photoelectrons correspond to VEx sampling a region of ionospheric plasma in the tail that is magnetically connected to the sunlit ionosphere. A similar observation has been seen at Titan (Coates *et al*., 2007).

5. Summary and conclusions

The presence of photoelectrons in the ionosphere of Venus can be inferred from their characteristic spectral shape in the electron population. Here, we present three case studies of photoelectron distributions observed by the ASPERA-4 instrument aboard Venus Express.

- The first case study, similar to the case presented by Coates *et al.* (2008), showed two peaks observed in the sunlit ionosphere corresponding to the theoretically expected (e.g. Mantas and Hanson, 1979) photoelectron spectrum with corresponding O^+ ions. This dawn-dusk pass showed that the photoelectron populations are observed on both

flanks of the planet and are not confined by orientation with respect to the planet's rotation.

- The second case study showed a photoelectron peak broadened in energy, possibly due to wave particle interactions between the source and observation point. The electrons could have been transported for enough time for pitch angle scattering to occur. The data in this case were from near the noon-midnight plane.

- The third case study represents the first clear observation of photoelectrons in the induced magnetotail of Venus. In this case we infer that VEx is in a region which has a magnetic connection to the sunlit ionosphere. The ELS pitch angles in the tail show near field-alignment. O^+ ions with energies up to ~60eV are seen in the vicinity. As at Mars and Titan, these photoelectron observations imply a possible role for the electrons in producing an ambipolar electric field which enhances ion escape.

- The directional information from ELS is limited by spacecraft obstructions; however, there are indications that the distributions are more field-aligned at higher altitudes and in the tail.

In addition to the electron observations, ions have been observed in the vicinity of photoelectrons in the dayside ionosphere (Case Study 1), in regions of ionospheric plasma seen in the tail (Case Study 2) and associated with ionospheric photoelectrons observed in the tail (Case Study 3). We interpret the latter observation as due to the location of VEx on a field line magnetically connected to the dayside ionosphere. This is the first time that ionospheric photoelectrons have been seen in the tail at Venus. They have been seen at Mars (Frahm *et al.*, 2006a,b) and Titan (Coates *et al.*, 2007).

In these cases, ionospheric electrons and relatively energetic photoelectrons may play a role in extracting ions from the ionosphere by ambipolar diffusion. The electrons are more mobile than ions allowing for creation of an electric field. The ions are then observed at the spacecraft either directly or with assistance of additional particle acceleration mechanisms (e.g., ion pickup). Comparing with the polar wind at Earth (e.g. Ganguli 1996, Yau et al., 2007 and references therein), an ambipolar field aligned potential of 1-2 eV may be set up, which would affect the observed energy of the photoelectrons. The photoelectrons are indeed shifted in energy, though this shift is likely dominated by the spacecraft potential; due to the ELS energy resolution it is not currently possible to separate the field aligned potential from the spacecraft potential, though this is an area for further study.

6. Acknowledgements

This work was supported by STFC in the UK; at Southwest Research Institute by NASA contract NASW-00003 in the USA; the Swedish National Space Board in Sweden. The authors thank Neville Shane for the analysis and plotting software. The ASPERA-4 team are grateful to NASA for allowing the ASPERA-3 ELS flight spare to be flown aboard VEx as part of ASPERA-4. It was constructed under contract NASW-00003.

The authors also wish to thank Tielong Zhang for the use of magnetometer data to produce the pitch angles for this study.

References

Barabash , S., *et al.*, The Analyser of Space Plasmas and Energetic Atoms (ASPERA-4) for the Venus Express mission, doi:10.1016/j.pss.2007.01.014, *Planet. Space Sci.*, *55*, 1772-1792, 2007.

Biernat, H.K., *et al.*, Aspects of MHD flow about Venus, *J. Geophys. Rev.*, *104*, 12,617-12,626, doi:10.1029/1999JA900032, 1999.

Biernat, H.K., *et al.*, MHD effects in the Venus magnetosheath, *Adv. Space Res.*, *26*, *10*, 1587-1591, doi:10.1016/S0273-1177(00)00085-5 ,2000.

Brace, L.H., and A.J. Kliore, The structure of the Venus ionosphere, *Space Sci. Rev.*, *55*, 81-163, doi:10.1007/BF00177136,1991.

Cloutier, P.A. and R.E. Daniell, Ionospheric currents induced by solar wind interaction with planetary atmospheres, *Planet. Space Sci.*, *21*, 463-474, doi:10.1016/0032-0633(73)90043-3, 1973.

Coates, A.J., *et al.*, Ionospheric photoelectrons observed in the magnetosphere at distances of up to 7 Earth radii, *Planet. Space Sci.*, *33*, 1267-1275, doi:10.1016/0032-0633(85)90005-4, 1985.

Coates, A.J., *et al.*, Ionospheric photoelectrons at Venus: Initial Observations by ASPERA-4, *Planet. Space Sci.*, *56*, 802-806, doi:10.1016/j.pss.2007.12.008, 2008.

Coates A.J., *et al.*, Ionospheric electrons in Titan's tail: plasma structure during the Cassini T9 encounter, *Geophys. Res. Lett.*, *34*, L24S05, doi:10.1029/2007GL030919, 2007.

Collinson, G. A., *et al.*, Electron optical study of the Venus Express ASPERA-4 Electron Spectrometer (ELS) top-hat electrostatic analyser, *Meas. Sci. Technol.., 20,* id:055204, doi: 10.1088/0957-0233/20/5/055204, 2009.

Cravens, T. E., *et al*., Model calculations of the dayside ionosphere of Venus: Energetics, *J. Geophys. Res., 85,* 7778-7786, doi: 10.1029/JA085iA13p07778, 1980.

Cui, J., M. Galand, A. J. Coates, T. L. Zhang, and I. C. F. M¨uller-Wodarg, Suprathermal electron spectra in the Venus ionosphere, J. Geophys. Res., 116, A04321, doi:10.1029/2010JA016153, 2011.

Davies, M.E., *et al.*, Report of the IAU Working Group on Cartographic Coordinates and Rotational Elements of the Planets and Satellites: 1985, *Celestial Mechanics, 39,* 103-113, doi:10.1007/BF01232291,1986.

Fazakerley, A.N., *et al.*, The Double Star plasma electron and current experiment, *Ann. Geophys., 23,* 2733-2756, doi:10.5194/angeo-23-2733-2005, 2005.

Fox, J. L., and S. W. Bougher, Structure, luminosity, and dynamics of the Venus thermosphere, *Space Sci. Rev., 55,* 357-489, doi:10.1007/BF00177141,1991.

Fox, J. L., and K. Y. Sung, Solar activity variations of the Venus thermosphere/ionosphere, *J. Geophys. Res., 106,* 21,305-21,335, doi:10.1029/2001JA000069, 2001.

Frahm, R.A., *et al.*, Locations of atmospheric photoelectron energy peaks within the Mars environment, *Space Sci. Rev., 126,* 389-402, doi:10.1007/s11214-006-9119-5, 2006a.

Frahm, R.A., *et al.*, Carbon dioxide photoelectron energy peaks at Mars, *Icarus, 182,* 371-382, doi:10.1016/j.icarus.2006.01.014, 2006b.

Frahm, R.A. *et al.*¸Estimation of the escape of photoelectrons from Mars in 2004 liberated by the ionization of carbon dioxide and atomic oxygen, *Icarus*, 206, 50-63, doi:10.1016/j.icarus.2009.03.024, 2009.

Ganguli, S. B., The polar wind, Rev. Geophys., 34, 311-348, doi: 10.1029/96RG00497, 1996.Gibson, E. G., *The Quiet Sun*, NASA SP-303, National Aeronautics and Space Administration, Washington, DC, 1973.

Jasperse, J. R., Electron distribution function and ion concentrations in the Earth's lower ionosphere from Boltzmann-Fokker-Planck theory, *Planet. Space Sci.*, *25*, 743-756, doi: 10.1016/0032-0633(77)90126-X, 1977.

Knudsen, W. C., *et al.*, Suprathermal electron energy distributions within the dayside Venus ionosphere, *J. Geophys. Res.*, *85*, 7754-7758, doi:10.1029/JA085iA13p07754,1980.

Law, C. C., and P. A. Cloutier, Observations of magnetic structure at the dayside ionopause of Venus, *J. Geophys. Res.*, *100*, 23,873-23,981, doi:10.1029/95JA02756, 1995.

Lewis, G.R., *et al.*, Derivation of density and temperature from the Cassini-Huygens CAPS Electron Spectrometer, *Planetary Space Science*, *56*, 7, 901-912, doi:10.1016/j.pss.2007.12.017, 2008.

Liemohn, M. W., et al., Numerical interpretation of high-altitude photoelectron observations, *Icarus*, *18*2, 383-395, doi:10.1016/j.icarus.2005.10.036, 2006.

Luhmann, J. G., and T. E. Cravens, Magnetic fields in the ionosphere of Venus, *Space Sci. Rev.*, *55*, 201-274, doi:10.1007/BF00177138, 1991.

Mantas, G.P. and W.B. Hanson, Photoelectron fluxes in the Martian ionosphere, *J. Geophys. Res.*, *84*, 369-385, doi:10.1029/JA084iA02p00369, 1979.

McCormick, P. T., P. F. Michelson, and D. W. Pettibone, On the energy deposition of photoelectrons in the atmosphere of Venus, *J. Geophys. Res., 81*, 5196-5200, doi: 10.1029/JA081i028p05196, 1976.

Padial, N., G. Csanak, B. V. McKoy, and P. W. Langhoff, Photoexcitation and ionization in carbon dioxide: Theoretical studies in the separated-channel static-exchange approximation, *Phys. Rev. A, 23*, 218-235, doi:10.1103/PhysRevA.23.218, 1981.

Phillips, J.L. and C.T. Russell, The upper limit on the intrinsic magnetic field of Venus, *J. Geophys. Res.*, *92*, 2253-2263, doi: 10.1029/JA092iA03p02253,1987.Russell, C.T., Elphic, R.C.and Slavin, J.A. Limits on the possible intrinsic magnetic field of Venus, *Journal of Geophysical Research*, 85, 8319-8332, doi:10.1029/JA085iA13p08319, 1980. Rymer, A., *et al*., Cassini Plasma Spectrometer Electron Spectrometer measurements during the Earth swing-by on August 18, 1999, *J. Geophys. Res.*, *106*, 30177-30198, doi: 10.1029/2001JA900087, 2001.

Schippers, P., *et al*., Identification of photoelectron energy peaks in Saturn's inner neutral torus,*J. Geophys. Res.*, 114, A12212, doi:10.1029/2009JA014368, 2009.

Slavin, J.A., *et al.*, The solar wind interaction with Venus: Pioneer Venus observations of the bow shock location and structure, *J. Geophys Res.*, *85*, 7625-7641, doi:10.1029/JA085iA13p07625, 1980.

Spenner, K., *et al.*, Photoelectron fluxes in the Venus dayside ionosphere, *J. Geophys. Res*., *102*, 2577-2583, doi:10.1029/96JA03341,1997.

Szita, S., *et al.*, Cluster PEACE observations of electrons of spacecraft origin, *Annales Geophysicae, 19*, 1721-1730, doi: 10.5194/angeo-19-1721-2001, 2001.

Titov, D.V., *et al*., Venus Express science planning, *Planet. Space Sci., 54*, 1279-1297, doi:10.1016/j.pss.2006.04.017, 2006.

Wei, H.Y., *et al.*, Cold ionospheric plasma in Titan's magnetotail, *Geophys. Res. Lett., 34*, L24S06, doi:10.1029/2007GL030701, 2007.

Whipple, E.C., Potentials of surfaces in space, *Reports on Progress in Physics*, *44*, 1197-1250, doi: 10.1088/0034-4885/44/11/002,1981.

Yau, A.W., T. Abe and W.K. Peterson, The polar wind: Recent observations, Journal of Atmospheric and Solar-Terrestrial Physics, 69, 1936–1983, doi:10.1016/j.jastp.2007.08.010, 2007.

Figure captions

Figure 1. Trajectory and spectrum for Case Study 1 (30 June 2006). **(a)** Orbit plot showing the VEx orbit in Venus Solar Orbital (VSO) co-ordinates during 29-30 June 2006. The Sun is to the left. In this and subsequent plots, outer and inner curves represent the nominal bow shock and ionopause, respectively (Biernat *et al.*, 1999,2000; Luhmann *et al.*, 1992). **(b)**. 20 electron spectra, in units of differential energy flux (DEF), are averaged from 01:54:08-01:55:28 UT on 30 June 2006. Error bars shown are Poissonian. The broad peak across the averaged spectrum is the ionospheric electron population. The prominent peaks towards the centre of the plot are due to ionospheric photoelectrons.

Figure 2. (a) Energy-time spectrogram of electrons in differential energy flux (DEF) for ELS anode 11 during 40 minutes on 30 June 2006. The differential energy flux is shown according to the colour scale on the right. The time resolution for the spectrogram is 4s. The photoelectron peaks are seen at 16eV and 21eV between 01:52 and 01:56 UT. **(b)** IMA ion data covering the same period (all sectors summed). **(c)** Spacecraft altitude. **(d)** Pitch angle distribution of O^+, at 01:50 UT, shown as the ion distribution function in the plane containing the magnetic field and velocity vectors. The distribution shows a low energy, 15.8km/s plasma flowing along the –B direction. **(e)** Composition data at 01:53 UT; vertical axis shows ion energy, horizontal axis is position of ions on the detector surface. Red curves correspond, from left to right, to O_2^+, O^+, He^+, H^+. Low energy O^+ is dominant during this period showing a peak below 20eV/q and slightly less than 40eV/q. The streak across the spectra between 20eV/q and 30eV/q is due to contamination by H^+.

Figure 3. (a) Orbit plot showing the VEx orbit during 03-04 June 2006; the format is the same as in Figure 1. **(b)** Electron spectra (20) of differential energy flux are averaged from 01:36:32-01:38:01 UT on 4 June 2006. The broad peak in each spectrum is due to the ionospheric electron population. **(c)** The second spectrum shows an ionospheric population in the tail region, averaged over 20 spectra between 01:52:45-01:54:09 UT.

Figure 4. Energy-time spectrogram of electrons in differential energy flux (DEF) for ELS anode 11 during 40 minutes on 4 June 2006, with other data in the same format as those shown in Figure 2(a)-(c). The photoelectron peaks are seen between 18eV and 19eV, between 01:36 and 01:42 UT and (less clearly) 01:52-01:54 and 01:55-01:57 UT. The ion pitch angle distributions **(d and e)** are shown in the same format as in Figure 2(d) at 01:39UT

and 01:55UT, respectively. Ion composition spectra **(panels (f) and (g))** are shown for similar periods, at 01:52 and 01:54 UT, and are in the same format as in Figure 2(e).

Figure 5. (a) Trajectory plot for 02-03 June, 2006. **(b)** Electron spectra (20) of differential energy flux averaged from 01:38:03-01:39:27 UT on 3 June. **(c)** spectra averaged over 01:55:00-01:56:28.

Figure 6. Data obtained during 40 minutes on 03 June 2006, in the same format as Figures 1 and 3. The photoelectron peaks are seen at 16 and 18eV between 01:38 and 01:46 UT plus at 01:55-01:57 UT (18eV) and 01:58-01:59 UT (18eV). Panels (d), (e), (f) and (g) are shown at 01:44, 01:47, 01:40 and 01:49 respectively.

First observations of ionospheric photoelectron peaks in the tail of Venus

At times the peaks are broadened, implying scattering

Indicates a magnetic connection between the observation point and the dayside ionosphere

Simultaneous ion observations support idea of an ambipolar electric field

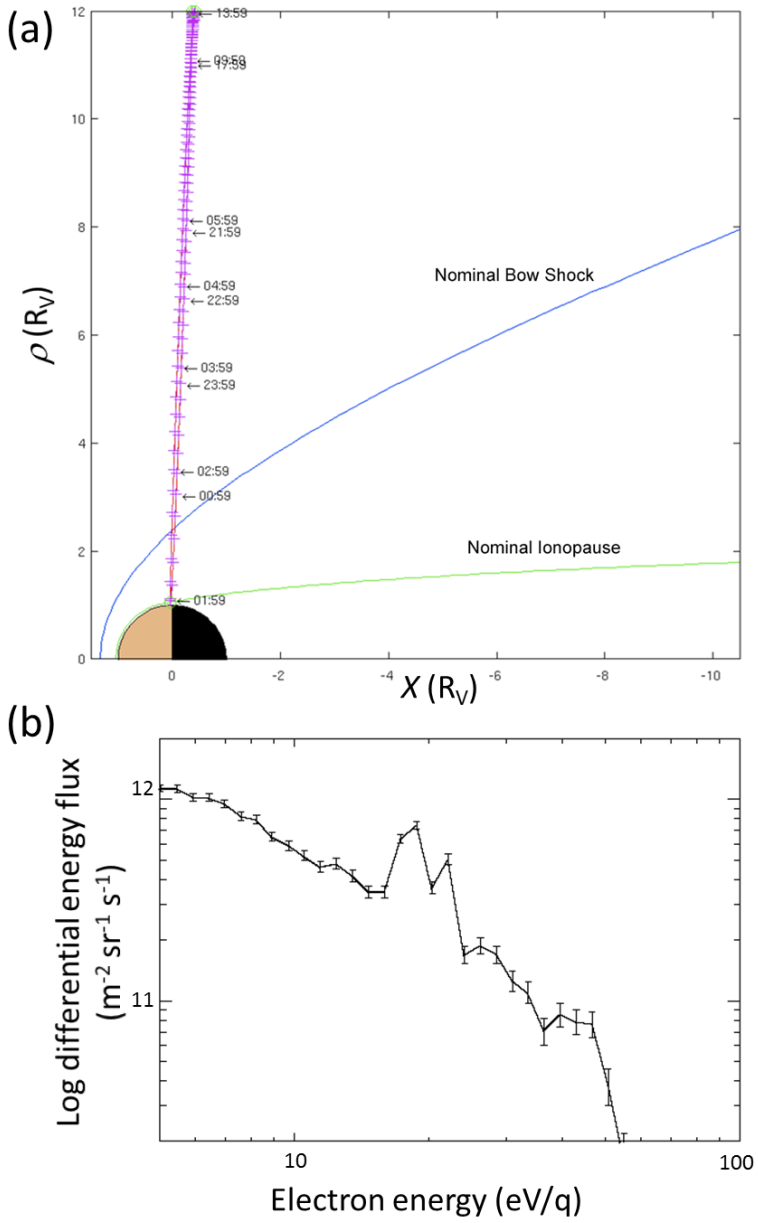

Figure 1. Trajectory and spectrum for Case Study 1 (30 June 2006). **(a)** Orbit plot showing the VEx orbit in Venus Solar Orbital (VSO) co-ordinates during 29-30 June 2006. The Sun is to the left. In this and subsequent plots, outer and inner curves represent the nominal bow shock and ionopause, respectively (Biernat *et al.*, 1999,2000; Luhmann *et al.*, 1992). **(b)**. 20 electron spectra, in units of differential energy flux, are averaged from 01:54:08-01:55:28 UT on 30 June 2006. Error bars shown are Poissonian. The broad peak across the averaged spectrum is the ionospheric electron population. The prominent peaks towards the centre of the plot are due to ionospheric photoelectrons.

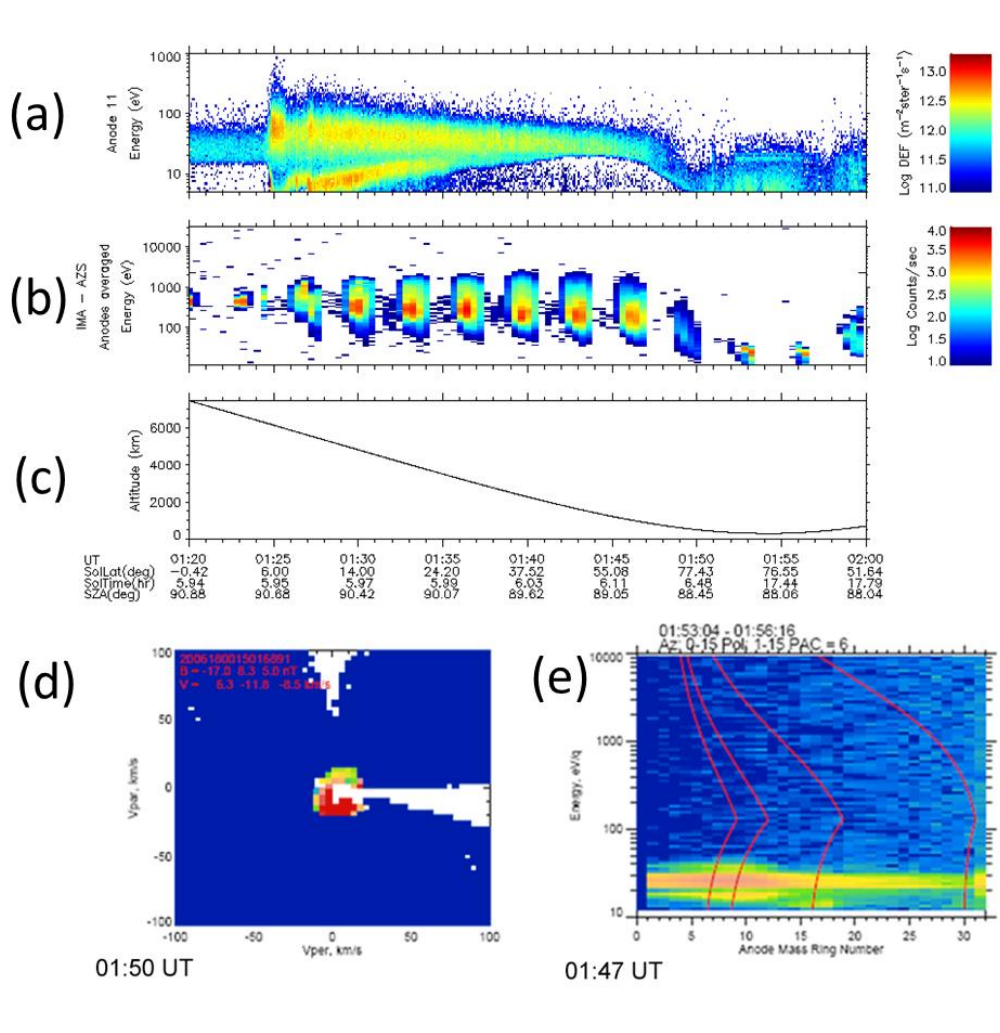

Figure 2. (a) Energy-time spectrogram of electrons in differential energy flux (DEF) for ELS anode 11 during 40 minutes on 30 June 2006. The differential energy flux is shown according to the colour scale on the right. The time resolution for the spectrogram is 4s. The photoelectron peaks are seen at 16eV and 21eV between 01:52 and 01:56 UT. **(b)** IMA ion data covering the same period (all sectors summed). **(c)** Spacecraft altitude. **(d)** Pitch angle distribution of O^+, shown as the ion distribution function in the plane containing the magnetic field and velocity vectors. The distribution shows a low energy, 15.8km/s plasma flowing along the –B direction. **(e)** Composition data; vertical axis shows ion energy, horizontal axis is position of ions on the detector surface. Red curves correspond, from left to right, to O_2^+, O^+, He^+, H^+. Low energy O^+ is dominant during this period showing a peak below 20eV/q and slightly less than 40eV/q. The streak across the spectra between 20eV/q and 30eV/q is due to contamination by H^+.

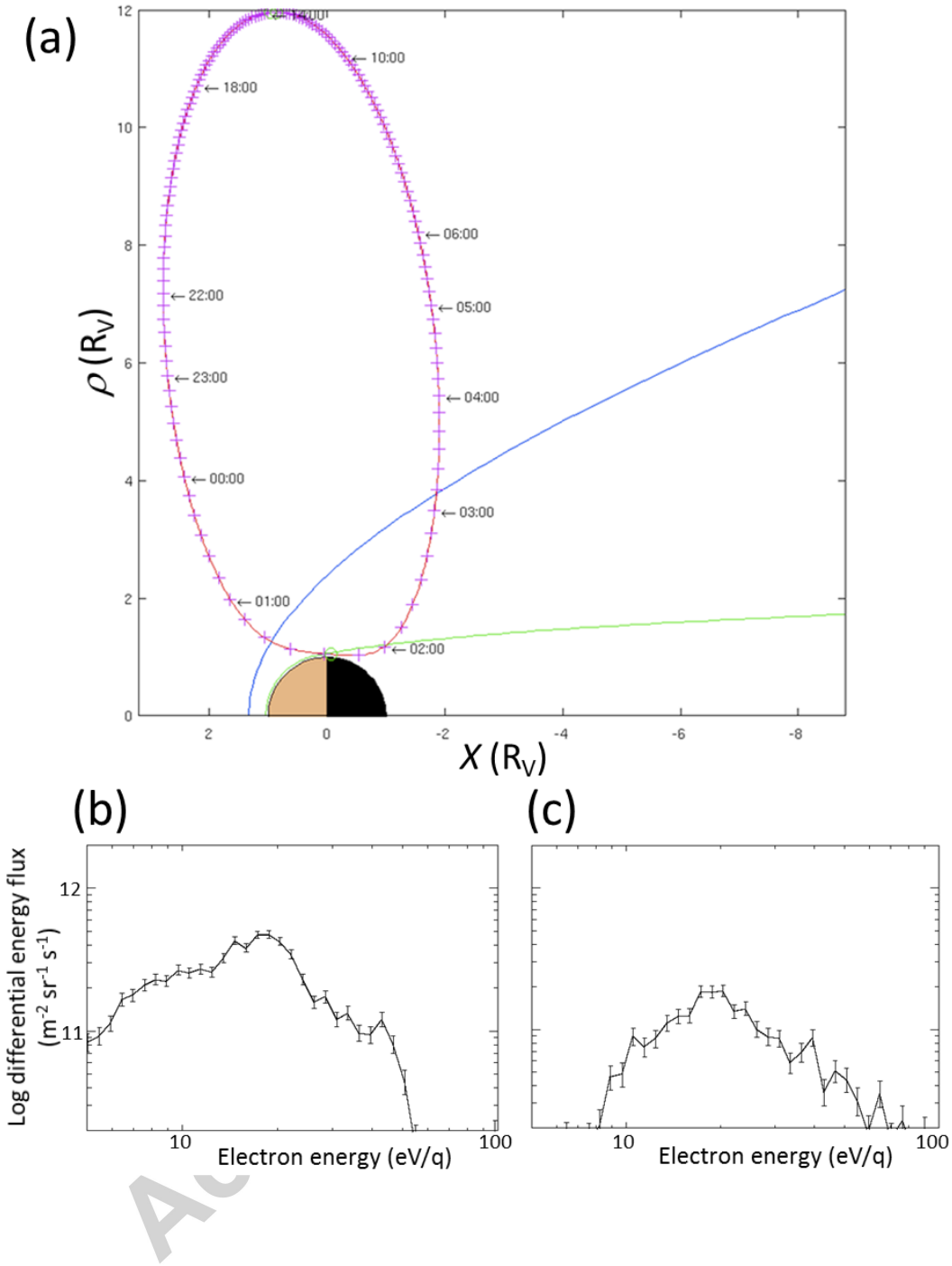

Figure 3. **(a)** Orbit plot showing the VEx orbit during 03-04 June 2006; the format is the same as in Figure 1. **(b)** Electron spectra (20) of differential energy flux are averaged from 01:36:32-01:38:01 UT on 4 June 2006. The broad peak in each spectrum is due to the ionospheric electron population. **(c)** The second spectrum shows an ionospheric population in the tail region, averaged over 20 spectra between 01:52:45-01:54:09 UT.

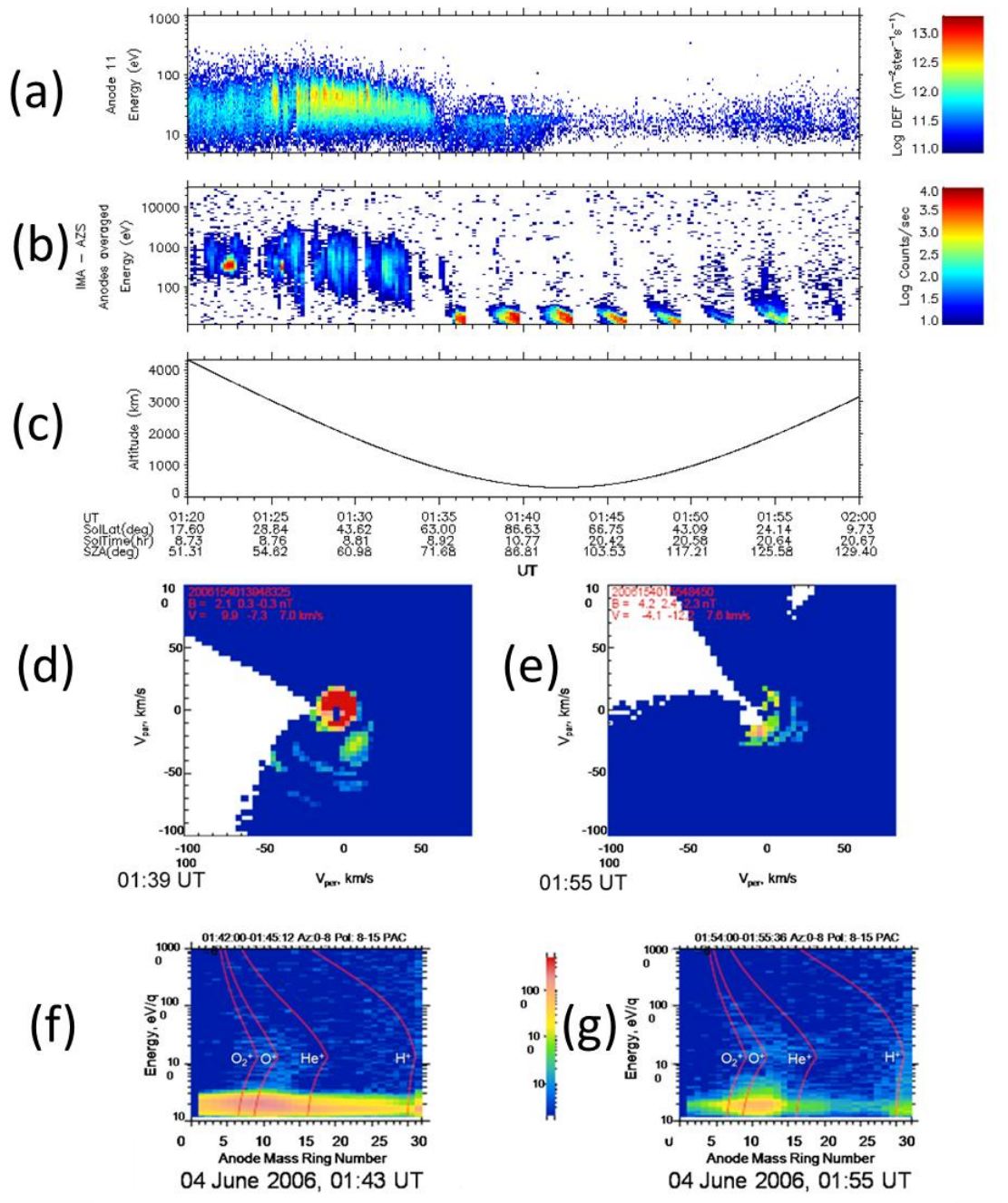

Figure 4. Energy-time spectrogram of electrons in differential energy flux (DEF) for ELS anode 11 during 40 minutes on 4 June 2006, with other data in the same format as those shown in Figure 2(a)-(c). The photoelectron peaks are seen between 18eV and 19eV, between 01:36 and 01:42 UT and (less clearly) 01:52-01:54 and 01:55-01:57 UT. The ion pitch angle distributions **(d and e)** are shown in the same format as in Figure 2(d) at 01:43UT and 01:55UT, respectively. Ion composition spectra **(panels (f) and (g))** are shown for the same two periods as in panels (d) and (e) above, and are in the same format as in Figure 2(e).

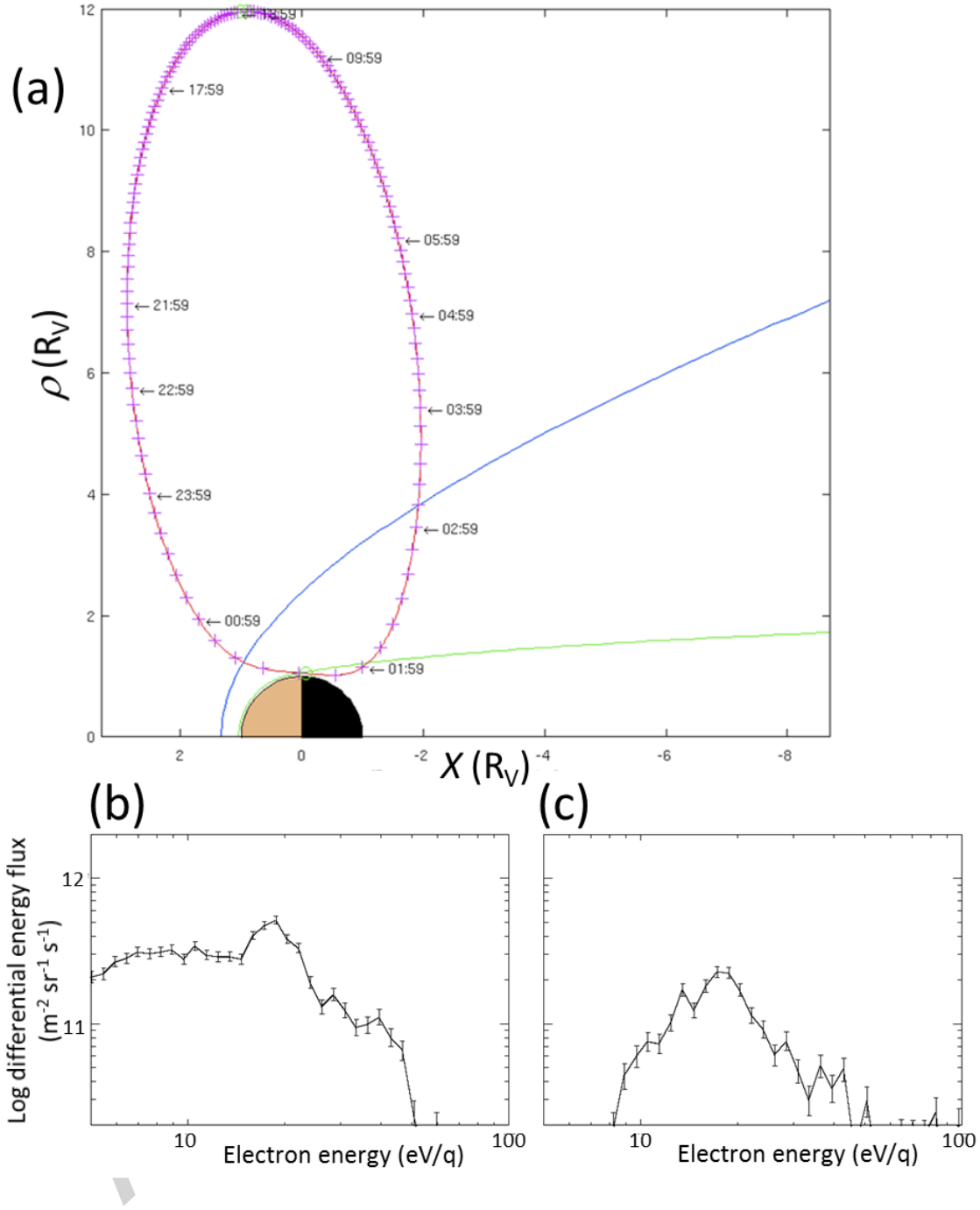

Figure 5. (a) Trajectory plot for 02-03 June, 2006. **(b)** Electron spectra (20) of differential energy flux averaged from 01:38:03-01:39:27 UT on 3 June. **(c)** spectra averaged over 01:55:00-01:56:28.

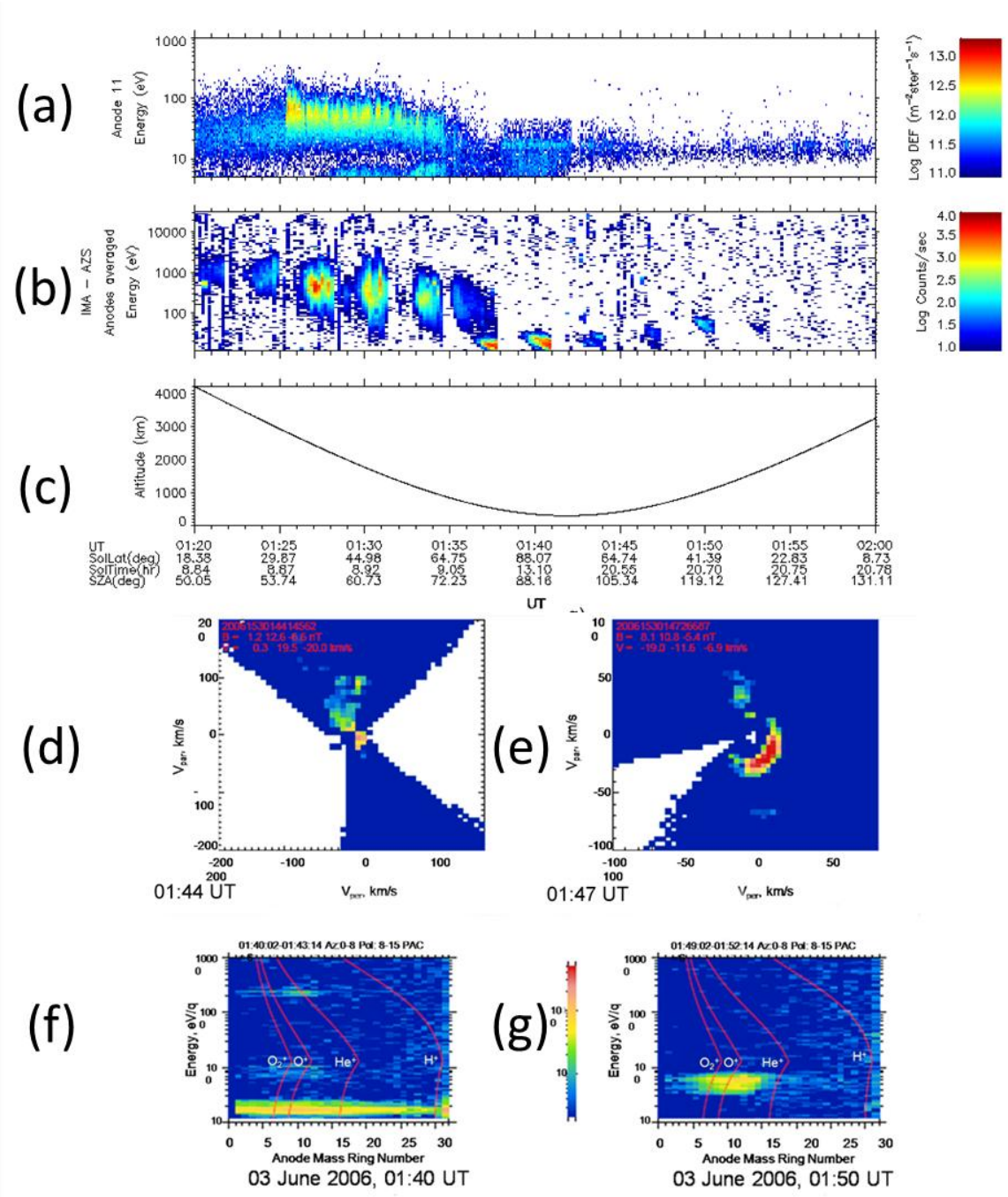

Figure 6. Data obtained during 40 minutes on 03 June 2006, in the same format as Figures 1 and 3. The photoelectron peaks are seen at 16 and 18eV between 01:38 and 01:46 UT plus at 01:55-01:57 UT (18eV) and 01:58-01:59 UT (18eV).